PERFORMANCE CHARACTERISTICS OF ROTATING, NON-CAPILLARY HEAT PIPES

Walter Hughes Newton, Jr.

United States
Naval Postgraduate School

THESIS

PERFORMANCE CHARACTERISTICS
OF
ROTATING, NON-CAPILLARY HEAT PIPES

by

Walter Hughes Newton, Jr.

Thesis Advisor: P.J. Marto

June 1971

Approved for public release; distribution unlimited.

Performance Characteristics of Rotating, Non-Capillary Heat Pipes

by

Walter Hughes Newton, Jr.
Lieutenant, United States Navy
B.S., United States Naval Academy, 1967

Submitted in partial fulfillment of the requirements for the degree of

MASTER OF SCIENCE IN MECHANICAL ENGINEERING

from the

NAVAL POSTGRADUATE SCHOOL
June 1971

ABSTRACT

A Nusselt-type analysis was performed for laminar film condensation on the inside of a rotating truncated cone with small half cone angles. This analysis included the interfacial shear between the vapor and condensate, the vapor pressure drop, the thermal resistance in the condenser wall, and the condenser outside cooling mechanism. An approximation of the analytical model made it possible to find a numerical solution for small half cone angles greater than zero.

A non-capillary rotating heat pipe containing an evaporator, condenser, and distilled water as the working fluid was tested. It was rotated at 702 and 1404 RPM, and the heat transfer rates of the heat pipe were determined experimentally for different saturation temperatures corresponding to electrical power inputs ranging from 1 kW to 9 kW.

The experimental results showed that the non-capillary rotating heat pipe was an effective heat transfer device. The approximate numerical solution conservatively predicted the heat transfer rate with a deviation of 18% at 702 RPM and 5% at 1404 RPM.

TABLE OF CONTENTS

TABLE OF SYMBOLS

A_c	surface area of condenser, ft^2
c_p	specific heat, Btu/lbm - °F
f	friction factor, dimensionless
h	heat transfer coefficient, Btu/hr - ft^2 - °F
h_{fg}	latent heat of evaporation, Btu/lbm
k_f	thermal conductivity of the liquid, Btu/hr - ft - °F
k_w	thermal conductivity of condenser wall, Btu/hr - ft - °F
L_c	length of condenser, ft
$\dot{m}$	mass flow rate of coolant, lbm/hr
p_v	pressure of the vapor, lbf/ft^2
P_{IN}	electrical power into evaporator, Btu/hr
Q_{EVAP}	heat transfer rate through the evaporator wall, Btu/hr
Q	theoretical heat transfer rate out of heat pipe, Btu/hr
Q_{OUT}	total experimental heat transfer rate out of heat pipe, Btu/hr
R	radius, ft
Re	Reynolds Number, dimensionless
T_s	saturation temperature, °F
T_w	outside condenser wall temperature, °F
T_∞	inlet coolant temperature, °F
t	condenser wall thickness, ft
u	velocity of liquid, ft/sec

v	velocity of vapor, ft/sec
w_f	mass flow rate of liquid, lbm/sec
w_v	mass flow rate of vapor, lbm/sec
x	coordinate measuring distance along condenser surface, ft
y	coordinate measuring distance normal to the condenser surface

GREEK

δ	film thickness, ft
ϕ	half cone angle, radians
ρ_f	density of the liquid, lbm/ft^3
ρ_v	density of the vapor, lbm/ft^3
τ	shear stress, lbf/ft^2
μ_f	viscosity of the liquid, lbm/ft - sec
μ_v	viscosity of the vapor, lbm/ft - sec
ω	angular velocity, rad/sec

ACKNOWLEDGEMENTS

The author would like to express his sincere appreciation to Dr. P.J. Marto of the Naval Postgraduate School for his guidance, advice, and constructive criticisms of this study as thesis advisor.

The author would also like to thank Michael O'Day and Don Harvey of the Naval Postgraduate School Machine Shop for their outstanding cooperation and enthusiasm and for the work they performed on machining various parts of the heat pipe.

Finally, the author wishes to thank his wife, Sandy, for her patience and assistance in the typing of the first draft.

I. INTRODUCTION

A. CONVENTIONAL HEAT PIPE

A heat pipe is a closed container capable of transferring large amounts of heat at nearly isothermal conditions. Conventionally it consists of four main parts: (1) evaporator, (2) condenser, (3) working fluid, and (4) capillary wicking structure to force the condensate back to the evaporator. The working fluid is evaporated in the evaporator section of the heat pipe by the heat source. As the vapor pressure increases, the vapor flows toward the condenser end, transporting the heat as the latent heat of vaporization. At the condenser end, the heat is removed from the vapor as it condenses. The condensate is then returned to the evaporator by the capillary pumping action within the wicking structure.

Studies of the heat transfer capabilities have been made on the conventional heat pipe [6, 10]* with the conclusion that, for ordinary fluids and moderate heat fluxes, the heat pipe is limited in its capability to transfer heat by the rate of condensate that can be returned to the evaporator.

B. THE ROTATING, NON-CAPILLARY HEAT PIPE

The rate of condensate flow may be increased by removing the wicking structure from the condenser. If the condenser

---

*Numbers in brackets indicate references listed in the bibliography.

end is then internally tapered and the heat pipe is rotated about its longitudinal axis, a centrifugal force field is set up which will overcome both the viscous losses in the system and the gravitational field.

Ballback's study [10] of the rotating heat pipe indicated that its heat transfer capability is limited by the amount of heat which can be removed from the condenser. In his study, Ballback performed a Nusselt-type analysis for the condensation on the inside of a truncated cone. In order to obtain a closed form approximate solution for the film thickness, δ, he made the following assumptions: (1) $\frac{d\delta}{dx} \ll \tan\phi$ (large cone angles), (2) no shear stresses between the vapor and condensate, and (3) no thermal resistance in the condenser wall. Daley [11] was able to improve on the theory introduced by Ballback by taking into consideration the thermal resistance in the condenser wall and the outside cooling mechanism. Furthermore, Daley neglected the assumption that $\frac{d\delta}{dx} \ll \tan\phi$. Using the velocity profile for the condensate developed by Ballback, he arrived at a non-linear second order differential equation for the film thickness, δ. Daley numerically integrated this expression using a Runge-Kutta-Gill numerical integration scheme with an IBM 360 MOD 67 digital computer. To start the integration, he used the conditions that $\delta = \delta i$ and $\frac{d\delta}{dx} = \tan\phi$ at $X = 0$. It was postulated that δi was a function of the over-fall condition at the step located at the condenser exit. Daley arrived at an expression for the minimum film thickness, δm,

at the condenser exit, using the approximation that the flow over the step approximated the free fall condition for open channel flow. Having found the film thickness from the second order differential equation at X = Lc, the condenser exit, Daley compared this value with δm at Lc. When the difference was less than .004, a solution was found. Using this technique, Daley was able to find the heat flow out of the condenser as a function of RPM for 0° half cone angle only. As the cone angle was increased, however, instability of the highly non-linear second order differential equation for the condensate film thickness caused the equation to be extremely sensitive to the initial value of the film thickness. Consequently, no solutions were found for the condensate film thickness for half cone angles greater than zero.

C. THESIS OBJECTIVES

The objectives of this study were to: (1) continue the theoretical study of the heat transfer capability of the rotating heat pipe and obtain solutions for $\phi > 0°$, (2) obtain experimental data from the heat pipe designed and assembled during Daley's study, and (3) compare the analytical and experimental results.

II. THEORETICAL PROGRAM

In order to improve on the analysis performed by Ballback and Daley the effects of vapor pressure drop and interfacial shear stress between the liquid and the vapor were included. Furthermore, the thermal resistance in the condenser wall and the outside cooling mechanism were considered. Using the coordinate system in Figure 1, for small half cone angles, momentum, continuity, and energy equations were developed for an infinitesimal fluid element. In addition, assuming one dimensional turbulent flow in the vapor, momentum and continuity equations were developed for the isothermal vapor flow.

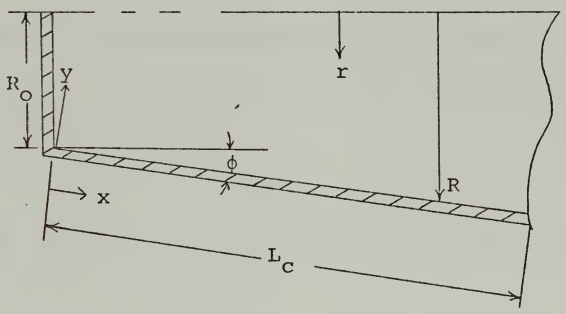

Figure 1. Coordinate system and geometry for condensate film analysis.

A. CONDENSATE MOMENTUM EQUATION (X-Direction)

By assuming that the momentum changes in the condensate are small a static force balance may be taken on an infinitesimal liquid element in the x-direction as shown in Figure 2.

$$0 = \frac{\partial \tau}{\partial y} - \frac{\partial p}{\partial x} + \rho_f \omega^2 \, r \sin \phi \qquad (1)$$

where

τ = shear stress

p = pressure

x = co-ordinate measuring distance along surface

y = co-ordinate measuring distance normal to surface

r = radius

ϕ = half cone angle

ρ_f = density of liquid

ω = angular velocity

B. CONDENSATE MOMENTUM EQUATION (Y-Direction)

Similarly, using Figure 2, a force balance in the Y-direction may be taken

$$0 = - \frac{\partial p}{\partial y} - \rho_f \omega^2 \, r \cos \phi \qquad (2)$$

Making use of Figure 2, the radius at any point in the fluid condensate may be expressed as:

$$r(x,y) = R_o + x \sin \phi - y \cos \phi \qquad (3)$$

where

R_o = minimum wall radius in the condenser section

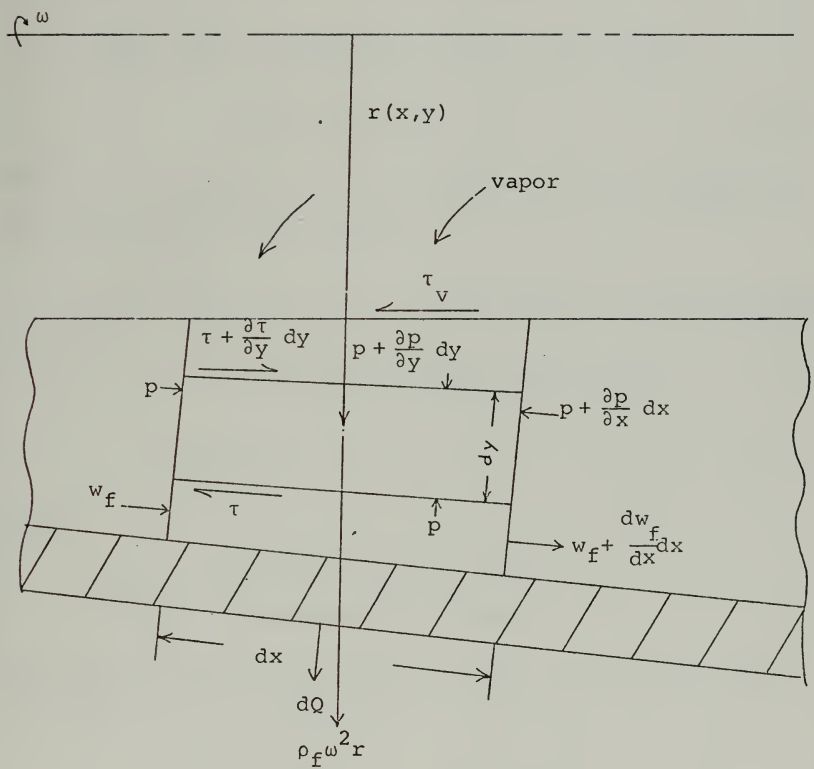

Figure 2. Cross-section of infinitesimal liquid element.

Substituting equation (3) for r(x,y) into (2), and integrating (2) from p to p_v and y to δ yields:

$$p(x,y) = p_v(x) + \rho_f \omega^2 \cos\phi\{(R_o + x\sin\phi)(\delta - y) - \frac{1}{2}\cos\phi(\delta^2 - y^2)\} \quad (4)$$

Differentiating equation (4) with respect to x gives

$$\frac{\partial p}{\partial x} = \frac{dp_v}{dx} + \rho_f \omega^2 \cos\phi\{(R_o + x\sin\phi - \delta\cos\phi)\frac{d\delta}{dx} + (\delta - y)\sin\phi\} \quad (5)$$

Substituting equation (5) into equation (1) and integrating from y to δ and τ to $-\tau_v$ gives

$$\tau = -\frac{dp_v}{dx}(\delta - y) - \tau_v - \rho_f \omega^2 \cos\phi\{(R_o + x\sin\phi - \delta\cos\phi)\frac{d\delta}{dx}(\delta - y)\} + \rho_f \omega^2 \sin\phi\{R_o + x\sin\phi - \delta\cos\phi\}(\delta - y)$$

$$= \mu_f \frac{\partial u(x,y)}{\partial y} \quad (6)$$

where

μ_f = viscosity of the liquid

u(x,y) = velocity of the liquid

Integrating equation (6) from 0 to y and from 0 to u gives an expression for the velocity of the fluid:

$$u(x,y) = -\frac{1}{\mu_f}\frac{dp_v}{dx}(\delta y - \frac{y^2}{2}) - \frac{\tau_v y}{\mu_f} + \frac{\rho_f \omega^2}{\mu_f}\left[R_o + x\sin\phi - \delta\cos\phi\right]\left[\sin\phi - \cos\phi\frac{d\delta}{dx}\right]\left[\delta y - \frac{y^2}{2}\right] \quad (7)$$

This expression for u(x,y) agrees with Ballback's except for the shear stress term.

C. CONTINUITY EQUATION

It is apparent from Figure 3 that due to the conservation of mass, with condensation

$$\frac{dw_f}{dx} = \frac{dw_v}{dx} \tag{10}$$

or

$$w_f = w_v \tag{10a}$$

where

w_f = mass flow rate of fluid

w_v = mass flow rate of vapor

The mass flow rate of the liquid may be written as

$$w_f = \int_o^\delta \rho_f u \, 2\pi r \, dy \tag{11}$$

The integrating of equation (11) using equations (3) and (7) yields

$$w_f = 2\pi\rho_f \{- \frac{1}{\mu_f} \frac{dp_v}{dx} [(R_o + x \sin\phi) \frac{\delta^3}{3} - \cos\phi \frac{5}{24} \delta^4]\}$$

$$+ 2\pi\rho_f \{- \frac{\tau_v}{\mu_f} [(R_o + x \sin\phi) \frac{\delta^2}{2} - \cos\phi \frac{\delta^3}{3}]\}$$

$$+ \frac{2\pi\rho_f^2\omega^2}{\mu_f} (R_o + x \sin\phi - \delta\cos\phi)(\sin\phi - \cos\phi \frac{d\delta}{dx})$$

$$[(R_o + x\sin\phi)\frac{\delta^3}{3} - \cos\phi \frac{5}{24} \delta^4] \tag{12}$$

The mass rate of flow of the vapor may also be written

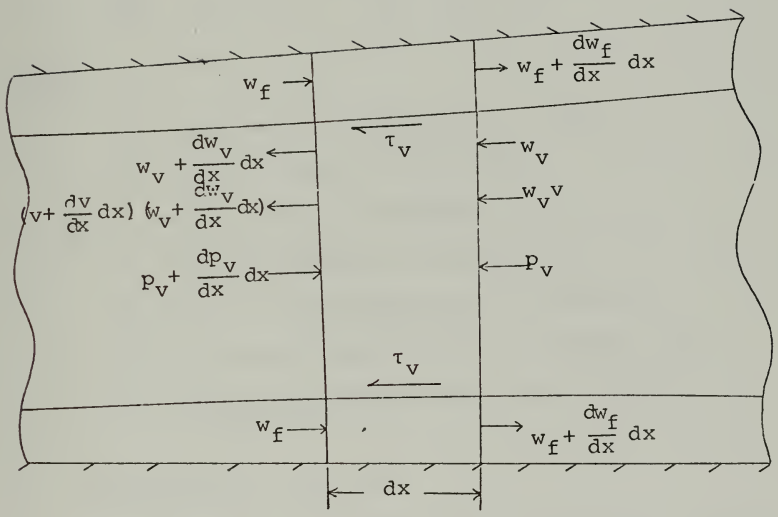

Figure 3. Cross section of infinitesimal liquid and vapor elements.

$$w_v = \rho_v \pi R^2 v \tag{13}$$

where

$$R = R_o + x \sin \phi - \delta \cos \phi$$

D. ENERGY EQUATION IN CONDENSATE

From Figure 2, using an energy balance, the rate of condensation may be written

$$\frac{dQ}{dx} = h_{fg} \frac{dw_f}{dx} = \frac{2\pi (R_o + x \sin \phi)(T_s - T_\infty)}{\frac{\delta}{k_f} + \frac{t}{k_w} + \frac{1}{h}} \tag{14}$$

where

T_s = saturation temperature of vapor

T_∞ = inlet coolant temperature

t = thickness of condenser wall

δ = film thickness of condensate

k_f = thermal conductivity of condensate

k_w = thermal conductivity of condenser wall

h = outside condenser wall heat transfer coefficient

E. VAPOR MOMENTUM EQUATION

Using Figure 3, and neglecting the momentum of the condensing vapor, a force balance may be taken in the x-direction.

$$p_v A - (p_v + dp_v)(A - dA) - (p_v + \frac{dp_v}{2}) dA - \tau_v dA_w$$

$$= (w_v + dw_v)(v + dv) - w_v v \tag{15}$$

where

p_v = pressure of vapor

v = velocity of vapor

A = cross sectional area of vapor element

A_w = surface area over which the shear stress acts

Neglecting higher order terms, and using the fact that $dA_w = 2\pi R dx$ equation (15) reduces to

$$\frac{dp_v}{dx} = - \rho_v v \frac{dv}{dx} - \frac{v}{\pi R^2} \frac{d}{dx} (w_v) + 2 \frac{\tau_v}{R} \qquad (16)$$

Using the expression $\tau_v = \frac{1}{2} \rho_v v^2 f$, where f = friction factor, and substituting into equation (16) yields

$$\frac{dp_v}{dx} = - \rho_v v \frac{dv}{dx} - \frac{v}{\pi R^2} \frac{d}{dx} (\rho_v \pi R^2 v) + \frac{\rho_v v^2 f}{R} \qquad (17)$$

Expanding the derivative in equation (17) yields

$$\frac{dp_v}{dx} = - 2\rho_v v \frac{dv}{dx} - \frac{2v^2 \rho_v}{R} \frac{dR}{dx} + \frac{\rho_v v^2 f}{R} \qquad (17a)$$

The first two terms in equation (17) represent the momentum effects of the vapor while the last term represents the usual friction effect. For the low condensate velocities which were expected during the experimental runs, according to Bergelin et al. [2] the friction factor is approximately equal to the friction factor used in smooth tubes (that is, the effect of the liquid film on the condenser surface is negligible). According to Rohsenow and Choi [3], the friction factor for turbulent flow in a smooth tube for vapor Reynolds numbers between 2000 and 50,000 is expressed as:

$$f = \frac{.0791}{(Re)^{\frac{1}{4}}} = \frac{.0791}{\left(\frac{2R\rho_v v}{\mu_v}\right)^{\frac{1}{4}}} \qquad (18)$$

F. DETERMINATION OF FILM THICKNESS AND HEAT TRANSFER RATE

Equations (10), (12), (13), (14), and (17a) can be further reduced to two simultaneous ordinary first order differential equations. Using equation (14) with the use of equations (10) and (13) for $\frac{dw_f}{dx}$ yields:

$$\frac{dv}{dx} = \frac{2(R_o + x\sin\phi)(T_s - T_\infty)}{\rho_v\left[\frac{\delta}{k_f} + \frac{t}{k_w} + \frac{1}{h}\right]R^2 h_{fg}} - \frac{2v}{R}\left[\sin\phi - \cos\phi\,\frac{d\delta}{dx}\right] \qquad (19)$$

At the same time, using equation (12) in conjunction with (10a) and (13) we obtain

$$\rho_v \pi R^2 v = 2\pi\rho_f\left\{-\frac{1}{\mu_f}\frac{dp_v}{dx}\left[(R_o + x\sin\phi)\frac{\delta^3}{3} - \cos\phi\,\frac{5}{24}\,\delta^4\right]\right\}$$

$$+ 2\pi\rho_f\left\{-\frac{\tau_v}{\mu_f}\left[(R_o + x\sin\phi)\,\frac{\delta^2}{2} - \cos\phi\,\frac{\delta^3}{3}\right]\right\}$$

$$+ \frac{2\pi\rho_f{}^2\omega^2}{\mu_f}(R_o + x\sin\phi - \delta\cos\phi)(\sin\phi - \cos\frac{d\delta}{dx})$$

$$\left[(R_o + x\sin\phi)\,\frac{\delta^3}{3} - \cos\phi\,\frac{5}{24}\,\delta^4\right] \qquad (20)$$

If equation (17a) is now substituted into equation (20), an equation for $\frac{d\delta}{dx}$ is obtained:

$$\frac{d\delta}{dx} = \tan\phi - \frac{\rho_v v^2 f\left[\frac{p_1}{R} + \frac{p_2}{2}\right] + \rho_v v\left[\frac{\mu_f R^2}{2\rho_f} - 2p_1\frac{dv}{dx}\right]}{p_1\cos\phi\left[\rho_f\omega^2 R + \frac{2\rho_v v^2}{R}\right]} \qquad (21)$$

where

$$p_1 = (R_o + x\sin\phi)\,\frac{\delta^3}{3} - \cos\phi\,\frac{5}{24}\,\delta^4$$

$$p_2 = (R_o + x\sin\phi)\,\frac{\delta^2}{2} - \cos\phi\,\frac{\delta^3}{3}$$

Equations (19) and (21) are two simultaneous first order ordinary differential equations with unknowns $\delta(x)$ and $v(x)$. A Runge-Kutta numerical integration was used to solve them with the IBM digital computer. It was hoped that by using first order differential equations rather than a second order, as Daley did, that the sensitivity to initial δ would be reduced. Figure 4 is a flow chart of the program used to solve the differential equations.

The integration was started by assuming initial conditions, $\delta=\delta_i$ and $v=0$ at $x=0$. With these initial conditions $\frac{d\delta}{dx} = \tan\phi$ at $x=0$. Figure 5 shows a schematic representing the calculated $\delta(x)$ for different initial values of δ. Note that if δ_i is too small the calculated δ becomes negative before the condenser overfall (physically impossible solution). If δ_i is too large the calculated δ grows at a constant slope equal to $\tan\phi$(physically unrealistic). With the proper choice of δ_i the calculated δ reaches a maximum along the length of the condenser and then tapers off to a value close to zero at the overfall. The exact value of δ at the overfall is not known. It was observed however that the calculated value of δ at the overfall was approximately .1 of δ_i, and the heat transfer rate was insensitive to an exact value at the overfall. This result agrees with Nimmo and Leppert [8] who experimentally found for laminar film condensation on a finite horizontal surface that the heat transfer rates were practically independent of the end conditions.

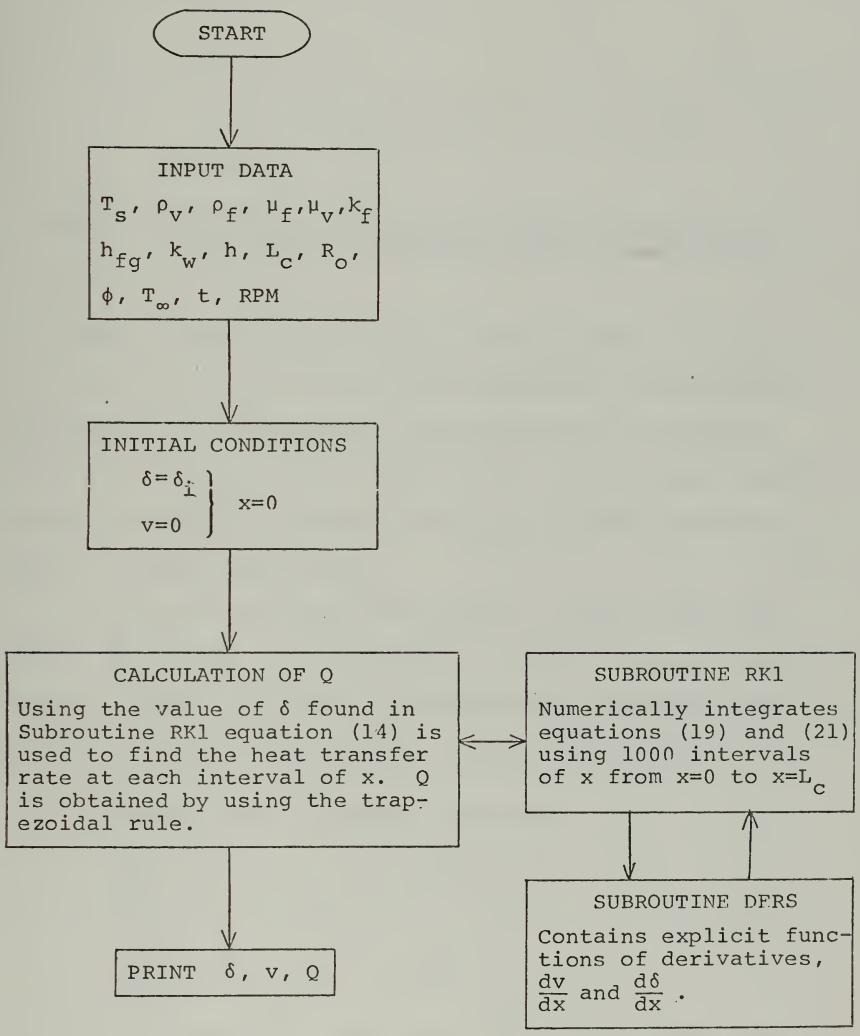

Figure 4. Flow chart of computer program.

$$\tan\phi \simeq \frac{\rho_v v^2 f\left[\frac{p_1}{R} + \frac{p_2}{2}\right] + \rho_v v\left[\frac{\mu_f R^2}{2\rho_f} - 2p_1\frac{dv}{dx}\right]}{p_1 \cos\phi\left[\rho_f\omega^2 R + \frac{2\rho_v v^2}{R}\right]} \tag{22}$$

$$\frac{dv}{dx} = \frac{2(R_o + x\sin\phi)(T_s - T_\infty)}{\rho_v\left[\frac{\delta}{k_f} + \frac{t}{k_w} + \frac{1}{h}\right] R^2 h_{fg}} - \frac{2v\sin\phi}{R} \tag{23}$$

Equation (22) may be further simplified by an order of magnitude analysis. Neglecting the second terms of p_1 and p_2 and using the expression, $R = R_o + x\sin\phi$ with the previously observed result that $p_1\frac{dv}{dx} << \frac{\mu_f R^2}{2\rho_f}$ and $\frac{p_1}{R} << \frac{p_2}{2}$, equation (22) may be rearranged in terms of a cubic equation for $\delta(x)$:

$$\frac{\delta^3}{3} R\sin\phi\left[\rho_f\omega^2 R + \frac{2\rho_v v^2}{R}\right] - \rho_v v^2 f\left[R\frac{\delta^2}{4}\right] - \rho_v v\frac{\mu_f R^2}{2\rho_f} = 0 \tag{24}$$

Equations (23) and (24) were solved simultaneously for $v(x)$ and $\delta(x)$. Equation (23) was numerically integrated using 1000 steps of integration over the cooling length of the condenser. The integration was started with initial conditions $\delta_i = 0$ and $v = 0$ at $x = 0$. Having found $v(x)$ at a particular step, equation (24) was solved by a subroutine. This value of δ was used to find $v(x)$ for the next step of integration. The results of approximation 1 are recorded in Table I for half cone angles of .1°, .2°, and .3°.

Using approximation 2 on equation (21), equation (24) was further simplified and rearranged to yield the following expression for $\delta(x)$:

TABLE I

THE HEAT FLOW, Q (Btu/hr), FOR
DIFFERENT HALF CONE ANGLES

ϕ	NUMERICAL SOLUTION Eqs. (19) & (21)	APPROXIMATE SOLUTION 1 Eqs. (23) & (24)	APPROXIMATE SOLUTION 2 Eqs. (23) & (25)
0°	8,505	-	-
.1°	10,082	9,836	10,290
.2°	11,173	11,033	11,332
.3°	11,904*	11,769	11,998

$$\delta(x) = \left[\frac{3\rho_v \mu_f v}{2\rho_f^2 \omega^2 \sin \phi}\right]^{1/3} \qquad (25)$$

Using equations (23) and (25) a numerical solution was found for $v(x)$ and $\delta(x)$ in the same manner as the solution for approximation 1. The results are tabulated in Table I for half cone angles of .1°, .2°, and .3°.

Table I shows that approximation 1 is lower than 2. This is to be expected since approximation 1 includes both interfacial shear between the vapor and condensate and the pressure drop in the vapor. At the same time approximation 1 is less than the more accurate solution of equations (19) and (21), thus giving a conservative result with a deviation

*In finding the solution for .3°, 10,000 steps were used in the integration. This was necessary because as the half cone angle became larger than .2°, the numerical integration became very sensitive to the step size.

of only 2.5%. Consequently, approximation 1 was used to arrive at a theoretical solution for $\delta(x)$ and Q for the one degree half cone angle condenser used in the experimental program. The results are plotted in Figures 9 and 10.

II. EXPERIMENTAL PROGRAM

A. DESCRIPTION OF EQUIPMENT

In order to facilitate the description of the entire experimental system, the system is sub-grouped into four parts: (1) evaporator, (2) condenser, (3) instrumentation, and (4) auxiliary equipment. Included in the description are drawings which are intended to aid the reader in visualizing the different components of the system. Figure 6 is a schematic representation of the entire system including the auxiliary equipment. Figure 7 is a cross-sectional drawing of the assembled heat pipe. Figure 8 is a photograph of the heat pipe and associated equipment.

1. Evaporator

The evaporator, modeled to approximate the rotating boiler tested at Lewis Research Center [17], is made of 304 stainless steel. It has an inside diameter of 3.125 inches, an outside diameter of 3.635 inches, an exit diameter of 2.625 inches, and an overall length of 5.905 inches.

The actual heated length is 3-7/8 inches around which an 11-gauge Chromel-A heater wire in a 3/16 inch inconel sheath is helically wound. The procedure of bonding the heater wire to the evaporator is an exacting process in order to ensure a uniform heat flux axially along the heater surface and to guard against electrical shorting between the heater wire and other components. The procedure was as follows:

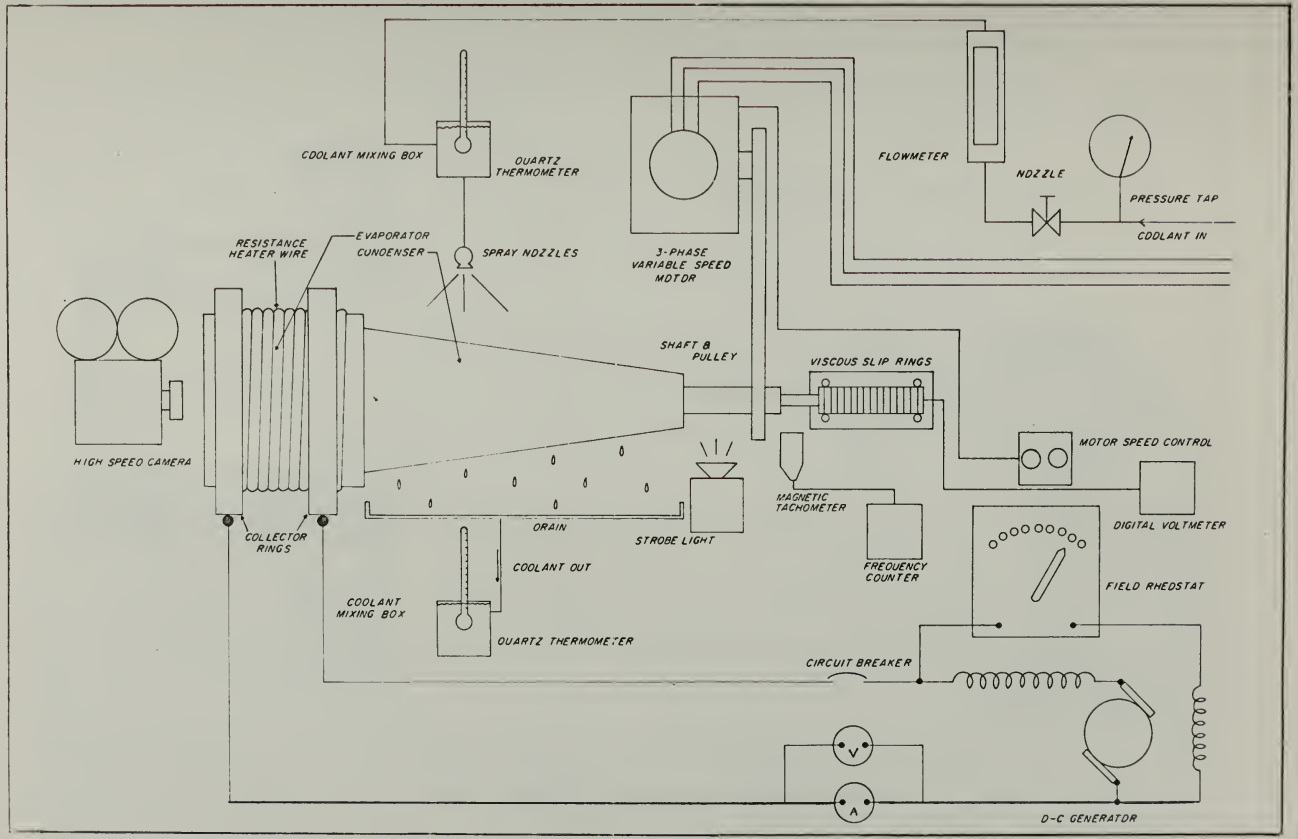

FIGURE 6 SCHEMATIC DIAGRAM OF APPARATUS

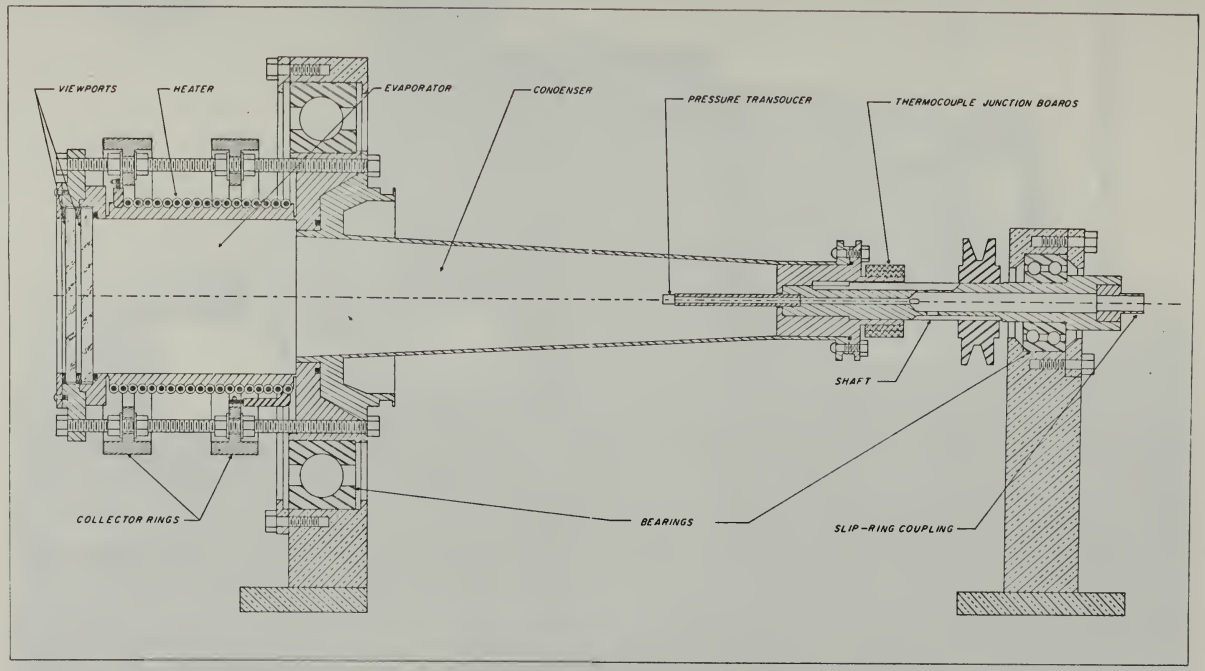

FIGURE 7 CROSS SECTION OF ROTATING HEAT PIPE

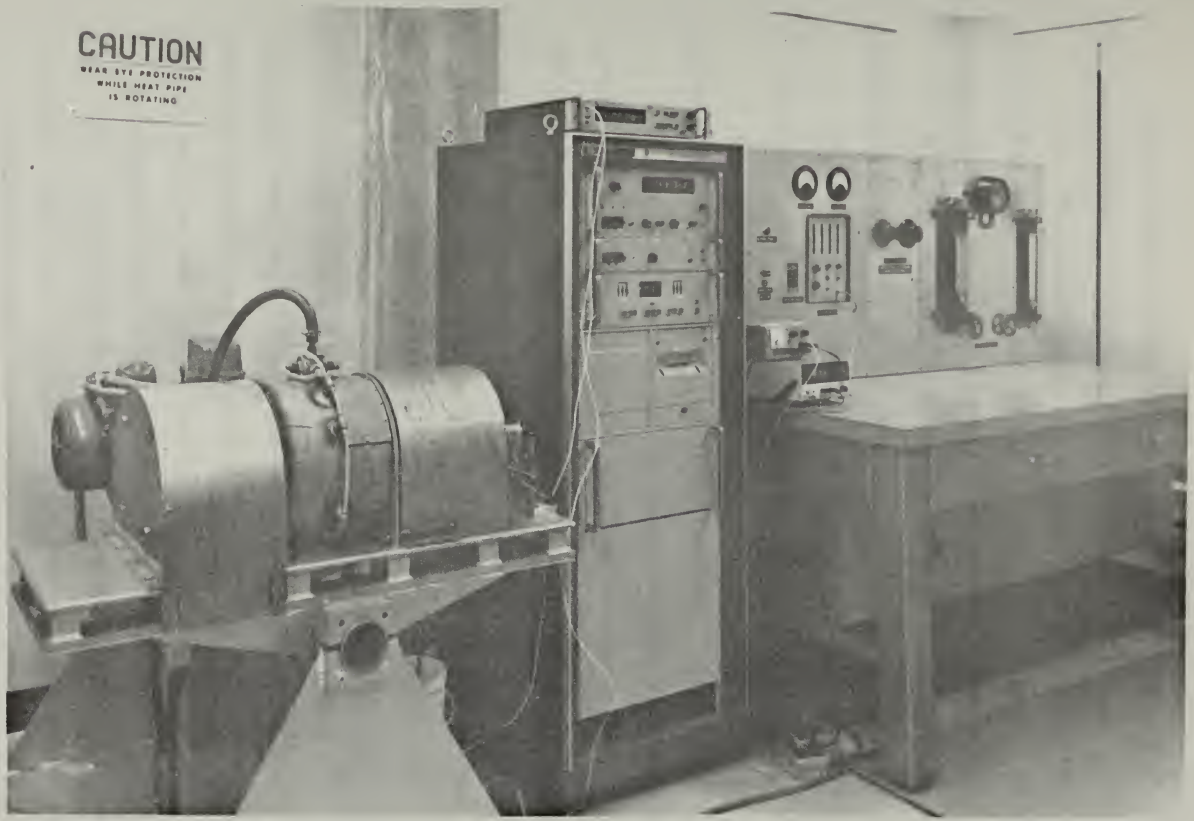

Figure 8. Photograph of heat pipe and associated equipment.

a. A sheet of gold-nickel foil, .003 inch thick, was tack welded to the outside evaporator surface.

b. The heater wire was helically wound over the gold-nickel sheet with two wraps of .020 inch diameter gold-nickel wire wound intermittently between the heater coils.

c. The assembly was then brazed in a hydrogen atmospherically-controlled oven.

d. Sauereisen cement was baked around the outside of the heater wire using the heater wire as the heat source.

e. Asbestos insulation was wrapped around the heater wire and tied off with glass tape.

f. Fish paper was placed into the heat sink on the condenser end of the evaporator to insulate the heater coils from the evaporator.

Power was furnished to the heater coils by a DC motor-generator capable of delivering 150 amperes at 220 volts. The electrical power was passed by a brush assembly consisting of eight spring-loaded graphite brushes through two bronze collector rings to the helically wound heater wire. The rings were supported by twelve 1/4 inch stud bolts. Phenolic spacers were used to align the collector rings and to insulate the bolts from the rings.

In order to reduce the axial heat losses, two radial 1/16 inch wide grooves were machined in the outside surface to within 1/16 inch of the inside boiler wall at either end of the heating element.

The outside face of the evaporator is closed by the insertion of two pyrex glass view ports, 3-1/2 inches in diameter. The inner view port rests on a neoprene O-ring seal and is separated from the outer view port by a 3/32 inch compressed fiber gasket. The view ports are held in place by a stainless steel end flange secured in place by twelve 1/4 inch stud bolts. The original design of two solid glass view ports was changed by fusing the inner view port to a glass tube which passes through the outer view port. This tube allows a vacuum to be drawn from the inside of the heat pipe during the filling procedure, and is easily sealed.

The inside diameter of the evaporator is stepped 1/2 inch from the exit diameter to allow for the formation of a liquid annulus in the evaporator.

2. Condenser

The condenser section is machined of stainless steel in the shape of a truncated cone. The half cone angle is 1°. The base of the condenser mates to the evaporator exit and has an inside diameter of 1.809 inches and tapers over a 10 inch length to a diameter of 1.460 inches at the truncated end. At this point, the condenser extends an additional 1-1/2 inches to house a cylindrical end plug.

A step is machined at the evaporator-condenser intersection where the condensate flows from the condenser to the recessed inside diameter of the evaporator. The first inch of the condenser surface near the evaporator is assumed to

be adiabatic and 9 inches of the condenser's overall length is considered as the cooling surface. The wall thickness of the condenser is 1/16 inch in order to reduce its thermal resistance.

The condenser section has two flanges. The large flange mates to the bearing seat flange on the evaporator and is held in place by the 1/4 inch stud bolts. The other flange mates to a flange on the end plug held together by eight 1/8 inch stud bolts. The end plug has an extension on its open end on which are mounted four phenolic junction boards.

3. Instrumentation

A schematic drawing of the instrumentation set-up is shown in Figure 6.

a. Temperature Measurements.

Temperature measurements are obtained from nine grounded copper-constantan thermocouples and two quartz thermometers. The thermometers are used to measure a temperature profile in the evaporator wall, the liquid annulus temperature in the evaporator, the vapor saturation temperature in the evaporator, the outside wall temperature of the condenser, and the temperature at the location of the pressure transducer.

In order to measure the temperature gradient in the evaporator wall, four thermocouples with a 1/16 inch diameter stainless steel sheath are utilized. Each thermocouple is placed within a 1/16 inch well drilled 3-1/2 inches deep into the evaporator wall. The thermocouple

junction is coated with epoxy to give it enough strength so that it will not bend when placed against the end of the well. The epoxy is sanded such that the junction makes contact with the wall.

One thermocouple is located 1/16 inch radially from the inside of the evaporator, another is located 1/16 inch radially in from the outside evaporator surface, and the remaining two are located opposite one another in the middle of the 1/4 inch wall at the same radial position to check on the uniformity of the temperature field.

The leads from all of the thermocouples in the evaporator wall are brought through slots in the evaporator and forward condenser flanges, down the side of the condenser, and through the rear condenser flange to phenolic junction boards. From the boards, the leads go inside the shaft and down to the slip ring unit which is attached to the main assembly by a coupling mounted at the end of the shaft.

A thermocouple is suspended in the liquid annulus to measure the liquid bath temperature. The remaining thermocouple in the evaporator is suspended in the vapor space to measure the saturation temperature.

Since these two thermocouples protrude into the inside of the heat pipe where a vacuum is held, precautions were taken to ensure that a seal was maintained. The ends of the two thermocouples were enclosed in stainless steel flanges and the leads were soldered at the slots on the condenser forward flange to keep air from passing through the slots into the evaporator.

In order to measure the outside condenser wall temperature, two thermocouples were soldered to grooves on the outside of the condenser at locations of 1/3 and 2/3 of its length respectively.

The remaining thermocouple was used to measure the temperature at the pressure transducer. The junction is soldered to the inside of the pressure transducer arm 1/32 inch from the surface.

The temperature of the coolant is measured before and after spraying by quartz thermometers mounted in mixing tubes located above and below the condenser spray cooling cylinder.

b. Pressure Measurements

The saturation pressure of the vapor at the small end of the condenser is measured by a semi-conductor pressure transducer mounted in the vapor space. The transducer is temperature compensated and is threaded on a 1/4 inch diameter arm that extends from the shaft through the end plug and about three inches into the vapor space. The leads of the probe pass through the transducer arm up through the shaft to the junction boards. From there, the leads pass back through the shaft to the slip ring unit.

c. Coolant Flow Rate Measurements

The coolant flow rate is measured by passing the coolant through a flow rotameter before the coolant enters the spray nozzles.

d. Rotational Speed Measurements

The rotational speed of the heat pipe is measured by two meters. A Beckman Eput Meter measures the RPM using a magnetic pickup, and an electronic strobe scope is used as a check.

e. Electrical Power Measurements

Power to the heater coils is measured by an ammeter and voltmeter connected in series and parallel respectively with the power lines returning from the heater. The power level is controlled by a field-rheostat placed in parallel with the DC motor-generator. A 150 ampere circuit breaker is included in the circuit.

f. Slip Ring Unit

The slip ring unit allows the rotating thermocouple leads and pressure transducer leads to pass electric current to stationary leads. The slip ring unit used in the experiment utilizes liquid mercury as a viscous contact medium between the rotating and stationary leads. The frictional heating noise is less than 10 microvolts at speeds up to 4000 RPM. The slip ring unit has 22 terminals to accommodate the nine thermocouples and pressure transducer. The output from the slip rings is fed to a Hewlett-Packard 2010C Data Acquisition System containing an integrating digital voltmeter, guarded data amplifier, and guarded cross-bar scanner. This system provides printed or visual output with an accuracy of ± .5 microvolts.

4. Auxiliary Equipment

The auxiliary equipment includes: (a) drive assembly, (b) test stand, (c) safety shields, and (d) spray assembly.

a. Drive Assembly

The drive assembly consists of a drive motor, end plug, shaft, pulley and bearing. The drive motor drives the shaft by means of a 2.65 inch diameter pulley and V-belt. The driving motor is a 2 horsepower, 3-phase variable speed motor capable of a maximum speed of 4000 RPM. The speed is controlled by a pushbutton electric remote control unit and the motor can be shut down instantaneously by a magnetic disc brake.

The end plug has a 3/4 inch threaded shaftway machined into it. Between the end plug and the shaftway is a .27 inch hole to allow for the insertion of the pressure transducer. The stainless steel shaft is hollow to allow for the passage of the thermocouple and the transducer leads to the slip ring unit. The shaft has 3/4 inch of its outside diameter threaded for screwing into the shaftway, and is threaded for 3/8 inch along its inside diameter on both ends. The condenser end mates with the transducer arm described earlier and the opposite end is joined to a coupling connected to the slip ring unit.

There are two main bearings supporting the heat pipe. The large, 5.96 inch diameter, floating, single bearing seats on the evaporator flange which is supported by an

aluminum pillow block. Copper cooling lines through which tap water flows have been placed in the pillow block to help cool the bearing. There is an oil input line at the top of the pillow block which allows for lubrication of the bearing. The small double row, angular contact bearing on the condenser end is mounted on a seat machined on the shaft and is self-lubricated.

b. Test Stand

The test stand was designed and built so that the heat pipe could be rigidly supported with its longitudinal axis ranging in position from 0 to 90 degrees from the horizontal. Both the heat pipe and variable drive motor are mounted on steel bed-plates connected by a 4 inch iron pipe. The iron pipe is held in place by three 2-inch thick clamps which are supported two feet off the ground by a 1/4 inch steel plate. As the heat pipe is rotated in any position, the drive motor rotates with it and the entire assembly is then securely held in place. The motor has been vibration mounted in order to keep the vibration to a minimum.

c. Spray Cooling Assembly

Cooling of the condenser section is done by spraying tap water on the outside of the condenser during rotation. The condenser section is enclosed by a 9-inch long 13-inch diameter stainless steel cylinder, the condenser box. The ends of the condenser box have Garlock rubber seals separating them from the condenser section.

The condenser box is slid into place over the condenser section through its open ends and is then bolted in place to the support plate. An 8-inch × 6-inch window has been cut in the condenser box in order to be able to make adjustments or repairs without removing the condenser box. During operation, a steel plate is bolted over the window. The condenser box has eight spray nozzles mounted at the same axial position. The nozzles may be varied to give a range of droplet sizes from 300 to 600 microns.

The coolant flows from copper feed lines to a mixing tube located at the top of the condenser box. A quartz thermometer records the temperature of the coolant in the tube. From the tube, the coolant flows through plastic tubing to each of the spray nozzles. The coolant drains from the bottom of the condenser box to another mixing tube where the temperature is recorded by the other quartz thermometer. From there the coolant flows to an external drain.

d. Safety Shields

During operation, the entire heat pipe assembly is surrounded by 1/8 inch thick stainless steel shielding bolted to the support plate to ensure safe operation.

The evaporator shield, shaped like an inverted U, is bolted to a 1.0 inch thick plexi-glass window on its open end. This window serves as a safety shield and also allows the internal pipe operation to be observed. The other end mates with the condenser box.

B. EXPERIMENTAL PROCEDURES

The experimental procedures consist of: (1) Filling Procedure and (2) Operational Procedure.

1. Filling Procedure

In order to obtain film condensation in the condenser, the inside surface of the condenser must be prepared so that proper "wetting" will take place during operation. The following procedure is used:

a. Scrub the condenser surface with 190°F Alconox detergent solution.

b. Flush with distilled water.

c. Spray with alcohol.

d. Rinse with distilled water.

e. Spray with acetone.

f. Rinse with distilled water.

Having completed the above procedure, the heat pipe is ready to be filled. In this study, distilled water was used as the working fluid.

In order to get a sufficient range of saturation temperatures and not exceed the 35 psia limit on the heat pipe, distilled water ice was placed in the evaporator and a low vacuum was drawn. The filling procedure was as follows:

a. System was cooled by circulating cooling water through the condenser nozzles and by inserting distilled water ice in the evaporator.

b. Six distilled water ice cubes (approximately 150 ml) were subcooled by flashing them with liquid N_2 and placed into the evaporator with tongs.

c. Glass windows were put into place and the flange was tightened with a 30 in-lb. torque.

d. The vacuum was drawn through the glass tube connected to a mechanical vacuum pump.

e. While the vacuum was being pumped, the glass tube was sealed using a gas flame.

2. Operational Procedure

Having completed the filling procedure, the heat pipe is ready to run at a pre-determined RPM. About 10 drops of lubricating oil are added to the oil fill tube at the top of the large pillow block. The cooling water lines are turned on so that the rotameter is at approximately 20% flow.

The drive motor is turned on and the heat pipe is slowly brought up to the desired RPM. Once a liquid annulus has formed in the evaporator and the desired RPM has been reached, the DC motor generator is turned on and power is added to the evaporator. Having reached thermal equilibrium for a particular power setting, data was taken by the instrumentation described earlier.

Shut-down is accomplished by first shutting off the current to the heater, and then decreasing the RPM by use of the remote control unit.

C. EXPERIMENTAL RESULTS

The heat pipe was run at 702 RPM and 1404 RPM. The run of 702 RPM was chosen because it was the lowest RPM at which

centrifugal forces dominated the gravitational effects. Power inputs to the heat pipe ranged from 1 kW to 9 kW.

1. Preliminary Results

Using distilled water as the working fluid, the heat pipe was rotated at 702 RPM to obtain the heat flow through the evaporator wall for a particular power setting. The method used to compute Q_{EVAP}, the heat flow through the evaporator wall, and the power supplied to the heater coils is shown in Appendix B. Table II shows a comparison between the electrical power into the heater coils and the heat flow through the evaporator wall for that particular power setting.

The data taken from the four thermocouples in the evaporator wall is obviously incorrect since part of the data shows that the heat flow through the evaporator wall is higher than the electrical heat in for that particular power setting. In other cases it appears to be low.

There are two explanations for the incorrect measurement of the heat flow through the evaporator wall. The first is the fact that the reading of thermocouple #2 appeared erratic. When the heat pipe is not rotating, thermocouple #2 appears to be reading correctly, but when the heat pipe rotates it begins to read inadequately. It was concluded that the problem existed in the slip ring and may be due to insufficient mercury in the slip ring. The second explanation pertains to the reason why the heat flow through the evaporator wall is higher than the heat into

TABLE II

POWER IN AND HEAT FLOW THROUGH EVAPORATOR WALL

POWER IN (BTU/HR)	HEAT FLOW IN EVAPORATOR WALL (BTU/HP)
3,345	4,059
6,712	10,315
9,963	12,848
13,325	7,610
16,988	9,126
20,751	24,041
24,031	13,437
27,278	31,986

the heater coils for a particular power setting. It was concluded that the outside edge coils on each side of the heating surface were conducting axially. As a consequence, there wasn't a uniform temperature distribution axially along the heating surface as assumed. Therefore, the actual heating surface length was less than the assumed length in the calculation of the heat flow and would account for the high values of the heat flow obtained in Table II.

At this point, it was decided to obtain the heat flow out of the heat pipe by performing an energy balance on the condenser cooling section. The coolant flow rate was determined by a flow rotameter, and its mean temperature was measured before and after spraying, by quartz thermometers

mounted in mixing tubes located above and below the condenser box. Having this information, along with the coolant's specific heat, the heat flow was determined by a simple energy balance. In order to make this method more accurate, the inside of the condenser box was insulated with silicone foam rubber and the plastic coolant lines were insulated with fiberglass. Appendix B contains a table showing the heat flow out of the condenser at different values of the heat pipe saturation temperature.

2. Visual Observations

Using a strobe light visual observations were made through the view ports. At 702 RPM, the light provided by the strobe light was insufficient. To increase the light, the strobe light's frequency was increased to three times the RPM of the heat pipe. As a consequence, the observations made at 702 RPM were not clear. The observation of the liquid vapor interface in the evaporator at low saturation pressures indicated violent boiling with large vapor bubbles breaking through the liquid vapor interface at 702 RPM. At higher saturation pressures, the boiling was more controlled with small bubbles constrained to the surface of the liquid. At the same saturation pressure, the boiling was less violent at 1404 RPM.

The visual observation in the condenser indicated that there were ripples and random break-up of the condensate film, exposing parts of the condenser surface to the vapor. Furthermore, the condensate swirled and washed the condenser

wall at a higher RPM than the wall itself. It is doubtful that the above observed effects were due to condensate turbulence. According to Rohsenow and Choi [3], in the presence of interfacial shear, turbulent condensate flow occurs for a Reynolds number between 100 and 1800. For the low vapor velocities which occurred during the observed experimental runs, the calculated transition Reynolds number in the condensate was approximately 1000. However, the highest Re calculated for the condensate was only 291. It was concluded, therefore, that the swirling and random film break-up were not caused by condensate turbulence but were probably caused by vapor interaction with the condensate.

Except for the 1 kW case, the Reynolds number calculated for the vapor flow for all of the power inputs was between 2000 and 9000 (for 1 kW, Re = 972). Since flow in a smooth tube is turbulent for Reynolds numbers between 2000 and 50,000 [3], it was concluded that the vapor flow was turbulent except for the 1 kW case. The swirling of the condensate was probably caused by the higher velocity vapor striking the condensate.

III. DISCUSSION OF RESULTS

The graphs in Figures 9 and 10 show the experimental and theoretical heat transfer rates as a function of the saturation temperatures (corresponding to an internal vapor pressure).

In order to find the theoretical values of the heat transfer rate, the value h, the heat transfer coefficient was needed. The method used in determining h is shown in Appendix B. Because of experimental uncertainties, the values of $h_{min} = 1000$ and $h_{max} = 1800$ were used since these values were very close to the average of the minimum and maximum experimental values of h determined for the different operating conditions.

As observed in Figure 9, the theoretical values of Q_{min} and Q_{max} are less than the experimental value of Q at 702 RPM. In the development of the analytical solution it was assumed that smooth film condensation occurred in the condenser. The visual observations described in the experimental results indicated that a smooth condensate film did not exist for the operating conditions used in these experiments but rather that the condensate film swirled and washed the condenser wall and appeared to break up in a random manner exposing part of the condenser surface to the vapor. The swirling effect and the resulting increased convection in the condensate increased the heat transfer

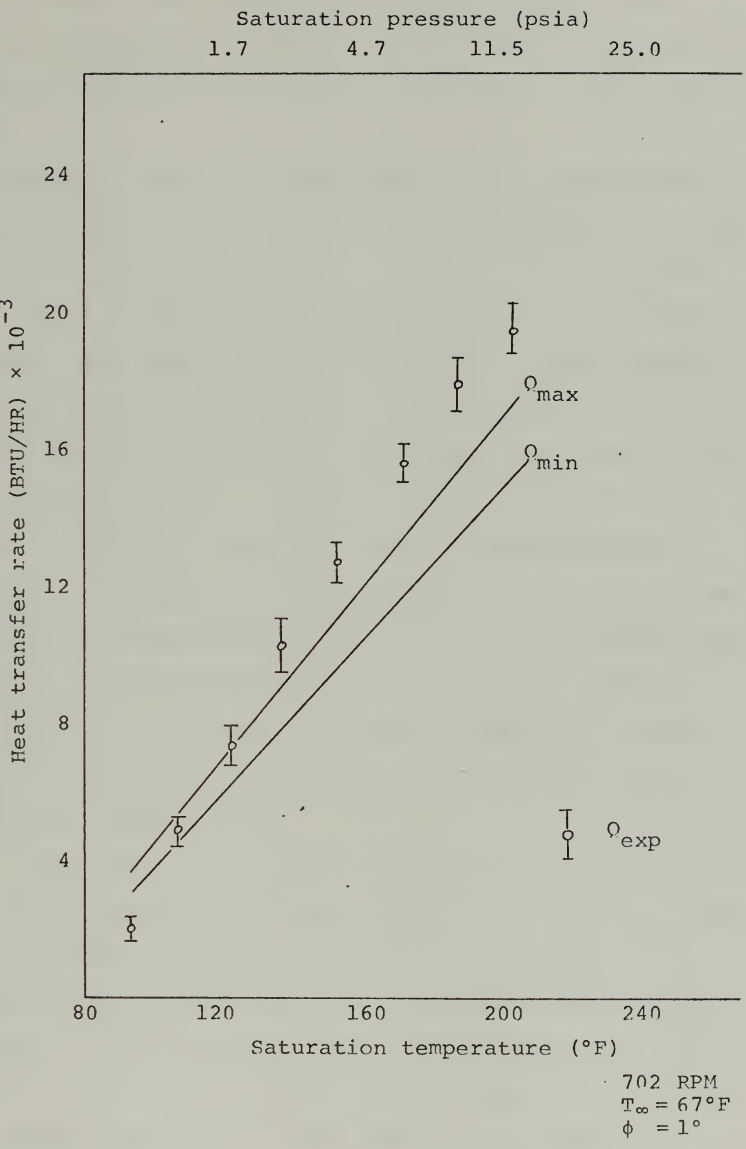

Figure 9. Heat transfer rate vs saturation temperature

rate. It was also possible that the ripples and film break-up decreased the overall film thickness, reducing the thermal resistance, and thereby increasing the heat transfer rate.

Figure 10 shows that the analytical and experimental results compare more favorably for the 1404 RPM run. There are two probable explanations. First of all, the higher RPM could have flattened the film causing it to approach a smoother film than in the 702 RPM run. If this were the case, the smooth film condensation assumptions would be better, and the analytical solution would be closer to the experimental results. Although the visual observations seemed to indicate that there were no non-condensibles present, the presence of non-condensibles in the condenser could be the second explanation. If non-condensibles were present, the experimental heat transfer curve would be shifted to the right since the heat transfer rate would require higher vapor pressures (and, therefore, higher saturation temperatures).

If the inlet coolant temperature were held constant, the heat transfer rate should increase with increased RPM for the same saturation temperature. For example, the analytical solution for Q_{min} at 1404 RPM at approximately the same T_{∞} used at 702 RPM resulted in higher heat transfer rates as shown by the dashed plot in Figure 10. Note that the experimental data at 1404 RPM does not appear to show an increase in heat transfer rates from the 702 RPM run.

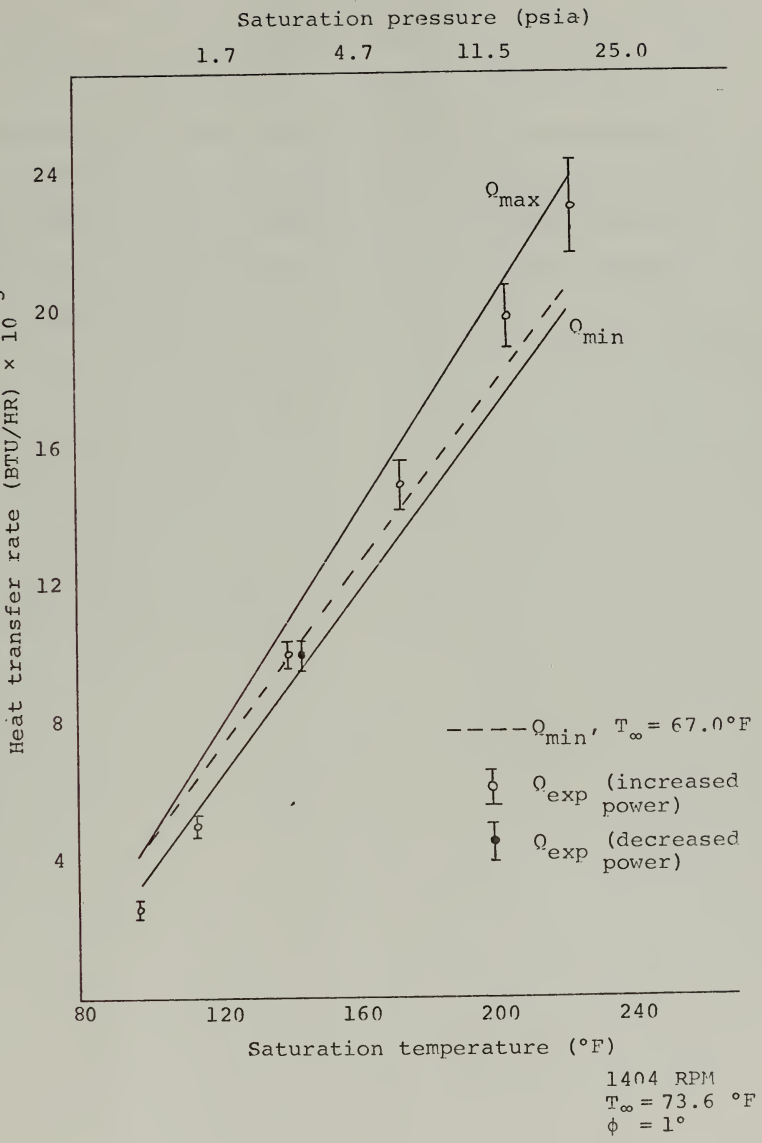

Figure 10. Heat transfer rate vs saturation temperature.

This is due to the fact that the 1404 RPM run was conducted at a higher T_∞ (7° difference) than the 702 RPM run. This increase in T_∞ increased the saturation temperature by approximately the same amount such that the experimental heat transfer rate data points were shifted to the right. At the same saturation temperature, therefore, the heat transfer rate was lower for the higher T_∞ even though it was at higher RPM.

IV. CONCLUSIONS AND RECOMMENDATIONS

A. CONCLUSIONS

1. The rotating non-capillary heat pipe is an effective heat transfer device.

2. Smooth film condensation was not observed during the experimental runs.

3. The approximate numerical solution conservatively predicts the heat transfer rate with a deviation of 18% at 702 RPM. The deviation of the numerical solution decreases to 5% for 1404 RPM.

4. The performance of the heat pipe is strongly dependent on the method used to cool the condenser.

B. RECOMMENDATIONS

1. Run the heat pipe at higher RPM to determine whether increased RPM provides better agreement between the analytical and experimental results.

2. Increase the instrumentation of the condenser to give more accurate data for the experimental heat transfer rate out of the condenser.

3. Revise the analytical solution to include the ripples and film break-up in the condenser.

4. Obtain experimental results for the effect of non-condensibles in the heat pipe.

5. Use different methods of cooling the condenser wall by using different spray nozzles.

6. Use a condenser section with a half-cone angle greater than 1° to obtain experimental data for the effect of larger cone angles on the heat transfer rate.

7. Use working fluids with boiling points lower than water in order to find optimum heat transfer rates at lower saturation temperatures.

APPENDIX A

CALIBRATION

1. Calibration of Pressure Transducer. The pressure transducer consists of a temperature-compensated, semiconductor strain gage Wheatstone bridge mounted on a 1/4-inch diameter diaphragm. It was calibrated against a Wallace-Tiernan standard pressure gauge (with a known accuracy of 0.03 ± 0.01 psia) for pressures greater than atmospheric, and against a mercury manometer (with an uncertainty of ±.02 psia) for pressures less than atmospheric. The transducer was calibrated at different operating temperatures by placing it within a controlled temperature oven with a quartz crystal thermometer (with an uncertainty better than ±0.1°F). Reproducible data was obtained from 0-30 psia and from 65-222°F, and the transducer sensitivity was measured to be 3.54 ± 0.06 mv/psia. Although the transducer Wheatstone bridge was temperature compensated, a non-linear zero shift with temperature was measured and incorporated into a series of calibration curves.

2. Calibration of Thermocouples. Nine 30 gauge, Kapton insulated, copper-constantan thermocouples were carefully manufactured at the Naval Postgraduate School. They were calibrated up to 384°F using the same temperature controlled oven and quartz crystal thermometer mentioned above. In

addition, the following fixed point calibrations were made:

a. Triple point of water (32.0°F)

b. Boiling point of water (212.0°F at 14.696 psia)

c. Melting point of tin (449.4°F)

d. Melting point of lead (621.3°F)

There were a total of nine calibration data points taken over the range of 32 - 621.3°F. Using the NBS table of calibration data for copper-constantan thermocouples as a zero reference, a deviation curve of the error (mv) vs. the thermocouple reading (mv) was plotted. This curve (with an uncertainty of 0.1%) was then used as a correction factor for each data point taken during the experiment before entering the NBS table for the temperature. Recalibration data was taken at a later time and the repeatability of all nine thermocouples was excellent. Using the boiling point of water and the melting point of tin, the deviation was within 0.005 mv of the previous data points.

3. Calibration of Rotameter. The method used in the calibration of the flow rotameter consisted of using a Toledo scale to measure the mass of the coolant flowing into a bucket placed on the scale. As coolant flowed into the bucket, an arbitrary starting point on the scale was taken and a stop watch was used to measure the time it took for the weight to reach 20 pounds. This procedure was repeated several times for each per cent flow rate used on the rotameter. Data points were obtained for 14, 16, 18 and 19.7 per cent flow rates. From this data a linear calibration curve was obtained.

APPENDIX B

DATA REDUCTION

1. Calculation of Q_{EVAP}

The heat flow through the evaporator wall may be reduced to a one dimensional steady state problem if it is assumed that there is no axial heat conduction and steady state conditions exist. Under these conditions, the well known conduction equation in cylindrical coordinates may be written [1]:

$$\frac{1}{r}\frac{d}{dr}\left(k(T)\, r \frac{dT}{dr}\right) = 0$$

or

$$k(T)\, r \frac{dT}{dr} = B = \text{Constant} \qquad (a)$$

where:

$$k(T) = k_o + m(T - T_o) \qquad (b)$$

A plot of k vs. T was made based on data taken from the Metals Handbook [5] for the thermal conductivity at different temperatures. From this plot the slope, m, and k_o were determined.

Substituting equation (b) into equation (a) and integrating yields:

$$F(T) = \left[k_o + m\left(\frac{T}{2} - T_o\right)\right] T = B \ln r + c_1$$

Using a sub-routine for the method of least squares, the IBM 360 computer was used to find the slope, B, of F(T) vs. ln r. From Fourier's law:

$$Q_{EVAP} = L\ 2\pi \left[k(t)\ r\ \frac{dT}{dr} \right]$$

or

$$Q_{EVAP} = L\ 2\pi\ B$$

where

L = the effective heating surface length in the evaporator

EXAMPLE: T_{SAT} = 153.7°F, 702 RPM

$$Q_{EVAP} = L\ 2\pi\ B$$

$L = .328$ (ft.)

$B = 4430.$ (BTU/hr - ft.)

$Q_{EVAP} = 9{,}126$ (BTU/hr)

2. Calculation of POWER IN

$$P_{IN} = \text{Voltage} \times \text{Current}$$

3. Calculation of Experimental Q_{OUT}

$$Q_{OUT} = \dot{m}\ C_p (T_1 - T_2)$$

where

$\dot{m}$ = mass flow rate (lbm/hr)

C_p = specific heat (BTU/lbm °F)

T_1 = inlet coolant temperature (°F)

T_2 = exit coolant temperature (°F)

Q_{OUT} = heat flow (BTU/hr)

EXAMPLE: TSAT = 153.72°F, 702 RPM

$\dot{m} = 797 \pm 18$

$C_p = 1.0$

$(T_1 - T_2) = 16.04 \pm 0.31$

$Q_{OUT} = 12{,}784 \pm 541$

4. Calculation of h, outside condenser wall heat transfer coefficient

$$Q_{OUT} = hA_c(T_w - T_\infty)$$

$$h = Q_{OUT}/A_c(T_w - T_\infty)$$

where

A_c = cooling surface area (ft^2)

T_w = outside wall temperature of condenser (°F)

T_∞ = coolant inlet temperature (°F)

h = heat transfer coefficient ($BTU/hr\text{-}ft^2\text{-}°F$)

EXAMPLE: TSAT = 153.72°, 702 RPM

$Q_{OUT} = 12{,}784 \pm 541$

$A_c = .34$

$(T_w - T_\infty) = 28.44 \pm 6.7$

$h = 1405 \pm 386$

5. Tables of Reduced Data

TSAT (°F)	$\dot{m}$ (LBM/HR)	$T_1 - T_2$ (°F)	$T_w - T_\infty$ (°F)	Q_{OUT} (BTU/HR)	h_{AVG} (BTU/HR-FT^2-°F)
			702 RPM		
93.4	835±23	3.06±.11	6.61± 1.8	2,555±165	1242±411
107.3	832±23	5.92±.25	11.1 ± 2.6	4,925±350	1403±423
122.8	804±20	9.23±.31	17.2 ± 2.7	7,421±440	1305±280
137.8	823±24	12.5 ±.54	22.9 ± 4.6	10,296±757	1388±375
153.8	797±18	16.0 ±.31	28.4 ± 6.7	12,784±541	1405±386
172.1	764±19	20.5 ±.25	34.1 ± 7.2	15,647±585	1417±350
188.3	764±19	23.6 ±.31	38.9 ±10.3	17,992±690	1515±465
204.4	863±19	22.6 ±.34	37.9 ± 8.5	19,538±730	1649±438
			1404 RPM		
98.4	870±23	3.02±.04	1.0 ±1.1	2,627±102	1225±408
115.3	850±24	5.96±.18	12.6 ±5.2	5,066±300	1445±664
141.8	825±22	12.2 ±.21	21.7 ±4.0	10,082±438	1417±320
174.3	790±20	18.9 ±.53	31.7 ±6.5	14.939±783	1456±371
205.6	786±27	25.4 ±.41	36.1 ±3.9	19,964±1011	1643±259
224.3	786±27	29.4 ±.68	45.6 ±9.0	23,132±1347	1563±395

BIBLIOGRAPHY

1. Chapman, A. J., Heat Transfer, pp. 49-50, MacMillan, 1967.

2. Bergelin, O. P., Heat Transfer and Fluid Mechanics Institute, Berkeley, California, 1949.

3. Rohsenow, W. and Choi, H., Heat, Mass, and Momentum Transfer, pp. 58-59.

4. Sparrow, E. M., and Hartnett, J. P., "Condensation on a Rotating Cone," Journal of Heat Transfer, Vol. 83, Series C, No. 1, pp. 101-102, February 1961.

5. Metals Handbook, 8th Edition, Vol. 1, American Society for Metals, 1961.

6. Katzoff, S., Notes on Heat Pipes and Vapor Chambers and Their Applications to Thermal Control of Spacecraft, Energy Commission/Sandia Laboratories Heat Pipe Conference, Vol. 1, October 1966.

7. National Aeronautics and Space Administration, NASA D-4136, Boiling Heat Transfer Coefficients, Interface Behavior, and Vapor Quality in Rotating Boiler Operating to 475 G's, by V. H. Gray, P. J. Marto, and A. W. Joslyn, March 1968.

8. Leppert, G. and Nimmo, B., Laminar Film Condensation on a Finite Horizontal Surface, paper presented at Fourth International Heat Transfer Conference, Paris, France, 31 August 1970.

9. Mosteller, W. L., The Effect of Nucleate Boiling on Heat Pipe Operation, M.S. Thesis, Naval Postgraduate School, Monterey, California, April 1969.

10. Ballback, L. J., The Operation of a Rotating Wickless Heat Pipe, M.S. Thesis, Naval Postgraduate School, Monterey, California, December 1969.

11. Daley, T. J., The Experimental Design and Operation of a Wickless Heat Pipe, M.S. Thesis, Naval Postgraduate School, Monterey, California, June 1970.

INITIAL DISTRIBUTION LIST

		No. Copies
1.	Defense Documentation Center Cameron Station Alexandria, Virginia 22314	2
2.	Library, Code 0212 Naval Postgraduate School Monterey, California 93940	2
3.	Assoc. Professor P. J. Marto Department of Mechanical Engineering Naval Postgraduate School Monterey, California 93940	4
4.	W. H. Newton 724 Alice Street Monterey, California 93940	1

UNCLASSIFIED

Security Classification

DOCUMENT CONTROL DATA - R & D

(Security classification of title, body of abstract and indexing annotation must be entered when the overall report is classified)

1. ORIGINATING ACTIVITY *(Corporate author)*

Naval Postgraduate School
Monterey, California 93940

2a. REPORT SECURITY CLASSIFICATION

Unclassified

2b. GROUP

3 REPORT TITLE

PERFORMANCE CHARACTERISTICS OF ROTATING, NON-CAPILLARY HEAT PIPES

4 DESCRIPTIVE NOTES *(Type of report and, inclusive dates)*

Master's Thesis; June 1971

5 AUTHOR(S) *(First name, middle initial, last name)*

Walter Hughes Newton, Jr., Lieutenant, United States Navy

6. REPORT DATE	7a. TOTAL NO. OF PAGES	7b. NO. OF REFS
June 1971	61	11

8a. CONTRACT OR GRANT NO.	9a. ORIGINATOR'S REPORT NUMBER(S)
b. PROJECT NO.	
c.	9b. OTHER REPORT NO(S) *(Any other numbers that may be assigned this report)*
d.	

10. DISTRIBUTION STATEMENT

Approved for public release; distribution unlimited.

11. SUPPLEMENTARY NOTES	12. SPONSORING MILITARY ACTIVITY
	Naval Postgraduate School Monterey, California 93940

13. ABSTRACT

A Nusselt-type analysis was performed for laminar film condensation on the inside of a rotating truncated cone with small half cone angles. This analysis included the interfacial shear between the vapor and condensate, the vapor pressure drop, the thermal resistance in the condenser wall, and the condenser outside cooling mechanism. An approximation of the analytical model made it possible to find a numerical solution for small half cone angles greater than zero.

A non-capillary rotating heat pipe containing an evaporator, condenser, and distilled water as the working fluid was tested. It was rotated at 702 and 1404 RPM, and the heat transfer rates of the heat pipe were determined experimentally for different saturation temperatures corresponding to electrical power inputs ranging from 1 kW to 9 kW.

The experimental results showed that the non-capillary rotating heat pipe was an effective heat transfer device. The approximate numerical solution conservatively predicted the heat transfer rate with a deviation of 18% at 702 RPM and 5% at 1404 RPM.

DD FORM 1 NOV 65 1473 (PAGE 1)

S/N 0101-807-6811

UNCLASSIFIED

Security Classification

KEY WORDS	LINK A		LINK B		LINK C	
	ROLE	WT	ROLE	WT	ROLE	WT
ROTATING HEAT PIPE						
FILM CONDENSATION						